Nanoscale Advances

ROYAL SOCIETY OF CHEMISTRY

PAPER

View Article Online
View Journal | View Issue

Check for updates

Cite this: *Nanoscale Adv.*, 2025, **7**, 1443

Band structure and magnetism engineering of InSe monolayers through doping with IVA- and VA-group atoms: role of impurities

Nguyen Thi Han,[a] J. Guerrero-Sanchez[b] and D. M. Hoat *[cd]

In this work, we investigate the electronic and magnetic properties of the InSe monolayer enriched by doping with IVA-group (Si and Ge) and VA-group (P and As) atoms. Both In and Se sublattices are considered as doping sites to realize n- and p-type doping (X_{In}@InSe and X_{Se}@InSe systems, X = Si, Ge, P, and As), respectively. The pristine InSe monolayer is an indirect gap semiconductor with a band gap of 1.41 eV. n-Doping processes preserve the monolayer's nonmagnetic nature. IVA-group impurities lead to monolayer metallization, while a considerable band gap reduction is induced by doping with VA-group atoms. The band gap also decreases considerably when realizing p-type doping with IVA-group atoms. In contrast, monolayer magnetization is achieved by p-type doping when replacing Se atoms with P and As atoms, leading to the formation of new 2D magnetic semiconductors. In these cases, VA-group impurities mainly produce the system's magnetism. Furthermore, our calculations also provide evidence for the emergence of magnetism in the InSe monolayer through doping with pair impurities (pX@InSe systems), where Si2/Ge2 (incorporated at the Se sublattice) and P1/As1 (incorporated at the In sublattice) dopant atoms play a key role in determining the electronic and magnetic properties of respective pair-atom-doped systems. Herein, the magnetic semiconductor nature of pSi@InSe and pGe@InSe systems is confirmed, while pAs@InSe is found to be a half-metallic system. Our results suggest the usefulness of doping with IVA- and VA-group atoms that can serve as an effective strategy to functionalize the InSe monolayer, providing insights into the role of impurities.

Received 5th December 2024
Accepted 4th January 2025

DOI: 10.1039/d4na01013b

rsc.li/nanoscale-advances

Open Access Article. Published on 23 Jänner 2025. Downloaded on 25.02.2026 06:53:42.
This article is licensed under a Creative Commons Attribution-NonCommercial 3.0 Unported Licence.

1. Introduction

In recent years, two-dimensional (2D) materials have attracted enormous attention because of their unique capabilities and properties. These materials form an important family that holds promise for diverse applications including electronics and optoelectronics,[1,2] photonics,[3,4] catalysis,[5,6] gas sensing,[7,8] biomedicine,[9,10] energy storage,[11,12] and environmental treatment,[13,14] among others. Undoubtedly, the most popular 2D material is graphene, an atom-thick hexagonal structure of carbon atoms arranged in a honeycomb configuration, which was obtained experimentally for the first time by Novoselov *et al.*[15] Remarkable properties have been found for graphene, such as strong mechanical and thermal stability, high thermal and electrical conductivity, chemical inertness, and high area surface,[16,17] among others. However, as a consequence of its zero band gap, the applications of graphene are considerably limited. Therefore, band gap opening is an important step that has been achieved by edge cutting[18] or surface functionalization.[19] Beyond graphene and its derivatives, many experimental and theoretical investigations have been performed in order to discover new 2D materials. In this regard, a wide variety of 2D materials have been presented, such as transition metal dichalcogenides – TMDs,[20,21] transition metal nitrides/carbides – also known as MXenes,[22,23] IVA-group and VA-group monoelementals and compounds,[24–27] III–V group compounds,[28,29] III–VI group compounds,[30,31] and so on.

Recently, increasing research attention has been devoted to 2D semiconductor IIIA-monochalcogenides both experimentally and theoretically. By using first-principles calculations, researchers have demonstrated the semiconductor nature of this 2D family, where the layer number is a determining factor for the band gap.[30,32] In their bulk counterparts, these materials crystallize in a layered structure, in which the layers are coupled to each other by weak van der Waals forces. Therefore, top–down methods can be used to thin down IIIA-monochalcogenides in order to form 2D crystals. For instance, Mudd *et al.*[33] carried out the successful exfoliation of InSe nanosheets with thickness down to a few manometers, which exhibit strong quantum confinement. Single and few-layered

[a]*Department of Basic Science, Hung Yen University of Technology and Education, Hung Yen, Vietnam*

[b]*Universidad Nacional Autónoma de México, Centro de Nanociencias y Nanotecnología, Apartado Postal 14, Ensenada, Baja California, Código Postal 22800, Mexico*

[c]*Institute of Theoretical and Applied Research, Duy Tan University, Ha Noi 100000, Vietnam. E-mail: dominhhoat@duytan.edu.vn*

[d]*Faculty of Natural Sciences, Duy Tan University, Da Nang 550000, Vietnam*

© 2025 The Author(s). Published by the Royal Society of Chemistry

Open Access Article. Published on 23 Jänner 2025. Downloaded on 25.02.2026 06:53:42.
This article is licensed under a Creative Commons Attribution-NonCommercial 3.0 Unported Licence.

InSe flakes have also been prepared by Petroni *et al.*[34] using the liquid-phase exfoliation. Characterization studies demonstrate the potential of the as-prepared materials for catalyzing the hydrogen evolution reaction. Moreover, 2D InSe layers have also been grown using bottom–up methods. Chang *et al.*[35] synthesized large-area InSe monolayers by chemical vapor deposition (CVD), which were further employed to fabricate n-type field-effect transistors with charge mobility up to ~30 $cm^2\ V^{-1}\ s^{-1}$ and an on/off ratio > $r_{bin}\ 10^4$ at room temperature. Alternatively, Zhou *et al.*[36] grew InSe monolayers with promising optoelectronic and photosensitive performance using physical vapor deposition (PVD).

Theoretically, several groups have investigated the effects of defects, doping, and atom adsorption on the InSe monolayer.[37–39] However, doping with IVA-group and VA-group atoms in InSe monolayers has not been investigated well, so far. Moreover, the role of impurities is also an important issue that should be clarified to provide deep insights into the effects of doping. In this work, our main aim is to propose effective methods to engineer the band structure and magnetism of InSe monolayers through doping with IVA-group (Si and Ge) and VA-group (P and As) atoms. It is found that the electronic and magnetic properties depend strongly on the doping site that presents either n-type doping (doping at the In sublattice) or p-type doping (doping at the Se sublattice).

2. Computational details

On the basis of density functional theory (DFT)[40] implemented in the Vienna *ab initio* Simulation Package (VASP),[41,42] first-principles calculations are performed employing the Perdew–Burke–Ernzerhof formalism within the generalized gradient approximation (GGA-PBE)[43] to describe the electron exchange–correlation potential. The pristine InSe monolayer is investigated using a unit cell containing 4 atoms, whose atomic structure can be constructed by cleaving the monolayer from the crystal structure of the bulk InSe compound.[44] In this case, the Brillouin zone is sampled with a Monkhorst–Pack special *k*-point mesh of 20 × 20 × 1.[45] A 4 × 4 × 1 supercell is used to study the doped InSe systems, with a *k*-grid size of 4 × 4 × 1. An energy cutoff of 500 eV is set in all calculations. For electronic self-consistency and ionic relaxation, the convergence criteria are set to 1×10^{-6} eV for energy and 1×10^{-2} eV $Å^{-1}$ for Hellmann–Feynman force, respectively. To prevent interactions between adjacent periodic layers (along the *z*-axis or perpendicular direction), a vacuum space (more than 14 Å) is introduced between them.

The formation energy E_f of the doped InSe monolayers is calculated using the following equations for the cases of doping at (1) the In sublattice, (2) the Se sublattice, and (3) the In + Se pair sublattices, respectively:

$$E_f = E(X_{In}@InSe) - E(InSe) + \mu_{In} - \mu_X \quad (1)$$

$$E_f = E(X_{Se}@InSe) - E(InSe) + \mu_{Se} - \mu_X \quad (2)$$

$$E_f = E(pX@InSe) - E(InSe) + \mu_{In} + \mu_{Se} - 2\mu_X \quad (3)$$

where $E(X_{In}@InSe)$, $E(X_{Se}@InSe)$, and $E(pX@InSe)$ are the total energy of the doped systems ($E(D@InSe)$); $E(InSe)$ denotes the total energy of the pristine InSe monolayer; μ_{In}, μ_{Se}, and μ_X refer to the chemical potentials of In, Se, and dopant X atoms (X = Si, Ge, P, and As), respectively. To verify their stability, cohesive energy E_c is computed as follows:

$$E_c = \frac{E(D@InSe) - n_{In}E(In) - n_{Se}E(Se) - n_XE(X)}{n_{In} + n_{Se} + n_X} \quad (4)$$

herein, the number of atoms A in the system and the energy of an isolated atom A are denoted by n_A and $E(A)$ (A = In, Se, and X), respectively.

3. Results and discussion

3.1 Pristine InSe monolayer

Fig. 1a shows the atomic arrangement of the InSe monolayer in its unit cell that contains two formula units (two vertically aligned In atoms between Se atoms in the atomic order: Se–In–In–Se). As a first step, we carried out the structural relaxation to get the optimized structure, which is characterized by the following parameters: (1) lattice constant a = 4.09 Å; (2) chemical bond lengths d_{In-Se} = 2.69 Å and d_{In-In} = 2.81 Å; (3) interatomic angles <SeInSe = 99.08° and <SeInIn = 118.53°; and (4) structural buckling height $\Delta = \Delta_{Se-In} + \Delta_{In-In} + \Delta_{In-Se}$ = 1.28 + 2.81 + 1.28 = 5.37 Å. The results are in good agreement with previous calculations of the InSe monolayer.[30,31] Moreover, they show good agreement with other calculations, for example, the lattice constant of the InSe monolayer is larger than that of the GaSe monolayer[30] or the InS monolayer[31] following the

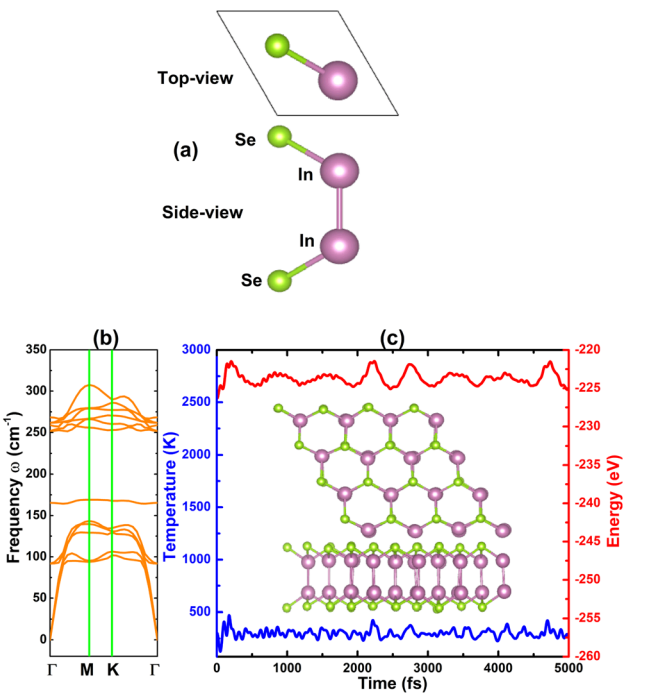

Fig. 1 (a) Visualization of a unit cell, (b) phonon dispersion curves, and (c) AIMD simulations at 300 K (final structure + variation of temperature and energy) of the InSe monolayer.

© 2025 The Author(s). Published by the Royal Society of Chemistry

Open Access Article. Published on 23 Jänner 2025. Downloaded on 25.02.2026 06:53:42.
This article is licensed under a Creative Commons Attribution-NonCommercial 3.0 Unported Licence.

criterion of atomic size. The stability of the InSe monolayer is now examined based on the following criteria:

• Cohesive energy E_c of the InSe monolayer is calculated from its unit cell using the following expression: $E_c = \frac{E(\mathrm{InSe}) - 2E(\mathrm{In}) - 2E(\mathrm{Se})}{4}$. A negative E_c value of −3.20 eV indicates good stabilization of the compound state of these 2D materials once formed.

• The dynamic stability of the InSe monolayer is checked through phonon dispersion spectra calculated with the PHONOPY code,[46] which is interfaced with density functional perturbation theory (DFPT). From the results plotted in Fig. 1b, no imaginary frequency is found in the whole spectrum, confirming that the InSe monolayer is dynamically stable.

• We then perform *ab initio* molecular dynamic (AIMD) simulations within the NVT ensemble using the Nose–Hoover method[47,48] to verify the thermal stability of the InSe monolayer at 300 K. To prevent the constraints imposed by periodic boundary conditions, a 4 × 4 × 1 supercell is adopted. From the results given in Fig. 1c, one can see stable fluctuation of temperature and energy. Moreover, the monolayer does not undergo remarkable structural distortion after 5000 fs of simulations. These results confirm that the InSe monolayer is thermally stable at room temperature.

According to our results of cohesive energy, phonon calculations, and AIMD simulations, the InSe monolayer has pronounced stability. Furthermore, we proceed to investigate its electronic properties through the band structure and projected density of states (PDOS). Considering the well known band gap underestimation of the GGA-PBE functional, we also calculate the band structure of the pristine InSe monolayer using the hybrid functional HSE06 to get a more accurate band gap.[49] From Fig. 2a, it can be concluded that the InSe monolayer is an indirect gap semiconductor as predicted by both employed functionals considering the valence band maximum along the

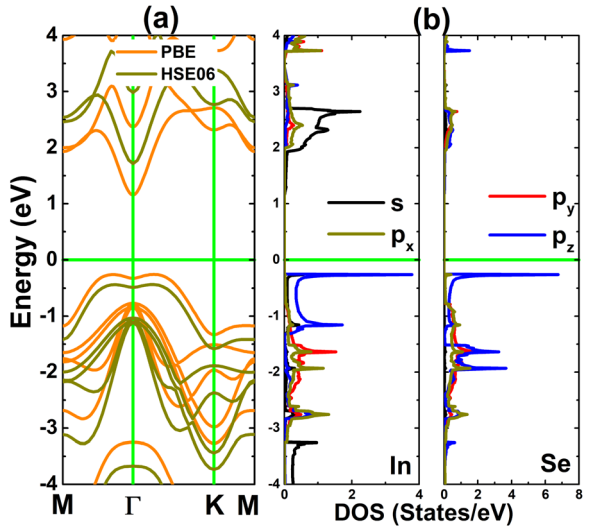

Fig. 2 (a) Electronic band structure and (b) projected density of states (calculated with the PBE functional) of the InSe monolayer (horizontal green line: the Fermi level is set to 0 eV).

ΓK path and the conduction band minimum at the *Γ* point. Our PBE- and HSE06-based calculations provide band gap values of 1.41 and 2.16 eV, respectively. PDOS spectra in Fig. 2b assert that the hybridization between In-p_z and Se-p_z states forms the upper part of the valence band, while the In-s state primarily forms the lower part of conduction band. The electronic hybridization may produce the covalent In–Se chemical bond. However, the difference in electronegativity between the In and Se atoms may also introduce an ionic character through charge transfer. Using Bader charge analysis, it is found that each In atom loses 0.63*e* of charge that move towards Se atoms.

3.2 Effects of doping at the In sublattice: n-type doping cases

In this part, the effects of doping with IVA- and VA-group atoms at the In sublattice on the InSe monolayer electronic and magnetic properties are investigated. In these cases, two- and one-electron n-type doping is realized, respectively, and we denote the doped systems as X_{In}@InSe (X = Si, Ge, P, and As). Applying eqn (1), E_f values of 1.41, 1.28, 2.28, and 1.69 eV are obtained for Si_{In}@InSe, Ge_{In}@InSe, P_{In}@InSe, and As_{In}@InSe systems, respectively. Note that Ge doping requires lower energy than other processes, demonstrating that it is easier to realize. Once formed, all X_{In}@InSe systems have negative E_c values between −3.21 and −3.18 eV per atom (see Table 1), which are similar to that of the pristine InSe monolayer, asserting their chemical-structural stability.

From our spin-polarized calculations, all four X_{In}@InSe systems have a zero magnetic moment, indicating that n-type doping preserves the nonmagnetic nature of the InSe monolayer. According to Bader charge analysis, Si, Ge, P, and As atoms transfer charge amounts of 1.13, 0.51, 0.13, and 0.31*e* to the host monolayer, respectively. The absence of magnetism in the doped InSe monolayers is also confirmed by the perfect overlap of spin-up and spin-down orbitals in the band structures displayed in Fig. 3. Importantly, new mid-gap states are induced by Si and Ge doping that extend through the Fermi level, leading to the monolayer metallization. Meanwhile, the results evidence the semiconductor nature of P_{In}@InSe and

Table 1 Formation energy E_f (eV), cohesive energy E_c (eV per atom), electronic band gap E_g (eV; spin-up/spin-down; M: metallic), charge transferred from impurity ΔQ (*e*; positive value: charge losing; negative value: charge gaining), and the total magnetic moment M_t (μ_B) of the doped InSe monolayer

	E_f	E_c	E_g	ΔQ	M_t
Si_{In}@InSe	1.41	−3.21	M/M	+1.13	0.00
Ge_{In}@InSe	1.28	−3.20	M/M	+0.51	0.00
P_{In}@InSe	2.28	−3.18	0.76/0.76	+0.13	0.00
As_{In}@InSe	1.69	−3.18	0.93/0.93	+0.31	0.00
Si_{Se}@InSe	3.01	−3.18	0.83/0.83	−0.16	0.00
Ge_{Se}@InSe	2.46	−3.17	0.83/0.83	−0.16	0.00
P_{Se}@InSe	1.70	−3.18	1.25/0.43	−0.58	1.00
As_{Se}@InSe	1.52	−3.17	1.25/0.39	−0.46	1.00
pSi@InSe	3.06	−3.21	0.86/0.95	+0.57/−0.04	1.00
pGe@InSe	2.56	−3.19	0.88/0.68	+0.28/−0.09	1.00
pP@InSe	2.75	−3.18	M/M	0.00/−0.39	0.81
pAs@InSe	2.32	−3.17	0.62/M	+0.15/−0.31	1.00

© 2025 The Author(s). Published by the Royal Society of Chemistry

Open Access Article. Published on 23 Jänner 2025. Downloaded on 25.02.2026 06:53:42.
This article is licensed under a Creative Commons Attribution-NonCommercial 3.0 Unported Licence.

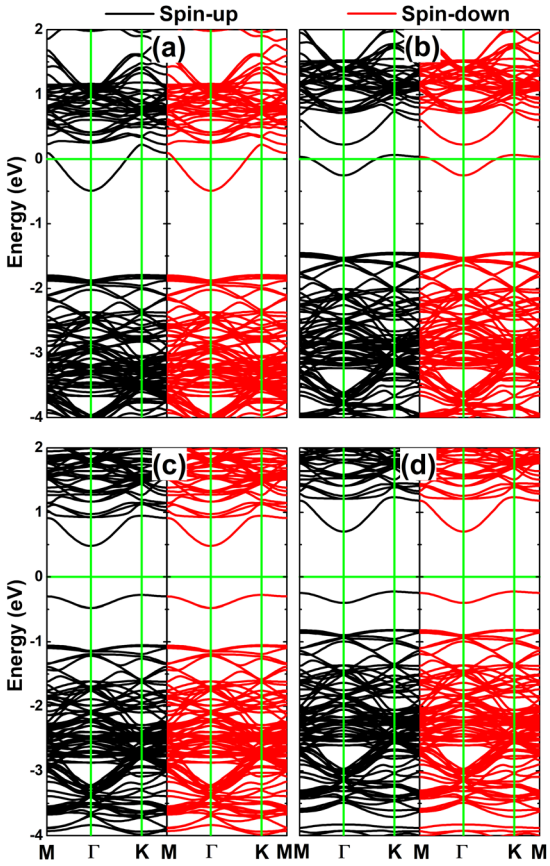

Fig. 3 Spin-polarized band structure of (a) Si_{In}@InSe, (b) Ge_{In}@InSe, (c) P_{In}@InSe, and (d) As_{In}@InSe monolayer (the Fermi level is set to 0 eV: green horizontal line).

As_{In}@InSe systems, whose band gaps are considerably smaller than that of the pristine InSe monolayer due to the appearance of mid-gap states. Specifically, these doped systems have energy gaps of 0.76 and 0.93 eV, respectively. Therefore, it can be concluded that n-type doping with P and As atoms leads to a band gap reduction on the order of 46.10% and 34.04% for the InSe monolayer, respectively. The band gap reduction may enhance the potential of the InSe monolayer for optoelectronic applications, widening the working region.

Fig. 4 shows the PDOS spectra of impurities and their first (Se) and second (In) nearest neighboring atoms to further study the origin of monolayer metallization and band gap reduction. In the Si_{In}@InSe and Ge_{In}@InSe systems, one can see that their metallic nature originates primarily from Si(Ge)-s and In-s states since they overlap with the Fermi level, where a small contribution from the Se-$p_{x,y}$ state is also confirmed. Meanwhile, the band gap reduction induced by P and As doping can be attributed to two main factors: (1) P(As)-s, In-p_z, and Se-$p_{x,y}$ states form mainly the mid-gap states below the Fermi level, and (2) P(As)-$p_{x,y}$ and In-s states make a new lower part of the conduction band. Furthermore, spin-up and spin-down states of all orbitals overlap perfectly to evidence again the nonmagnetic nature of X_{In}@InSe systems.

3.3 Effects of doping at the Se sublattice: p-type doping cases

Herein, we investigate the electronic and magnetic properties of X_{Se}@InSe systems (X = Si, Ge, P, and As), which are formed by doping with X atoms at the Se sublattice to realize p-type doping processes. Applying eqn (2), formation energies of 3.01, 2.46, 1.70, and 1.52 eV are obtained for Si_{Se}@InSe, Ge_{Se}@InSe, P_{Se}@InSe, and As_{Se}@InSe systems, respectively. These results evidence that As doping is easier to achieve, requiring less energy than other processes. It is important to mention that IVA-group impurities may prefer to be doped at the In sublattice rather than the Se sublattice, considering smaller E_f values of Si_{In}@InSe/Ge_{In}@InSe systems in comparison with Si_{Se}@InSe/Ge_{Se}@InSe systems. In contrast, the Se site is the preferred doping site for VA-group impurities as confirmed by the

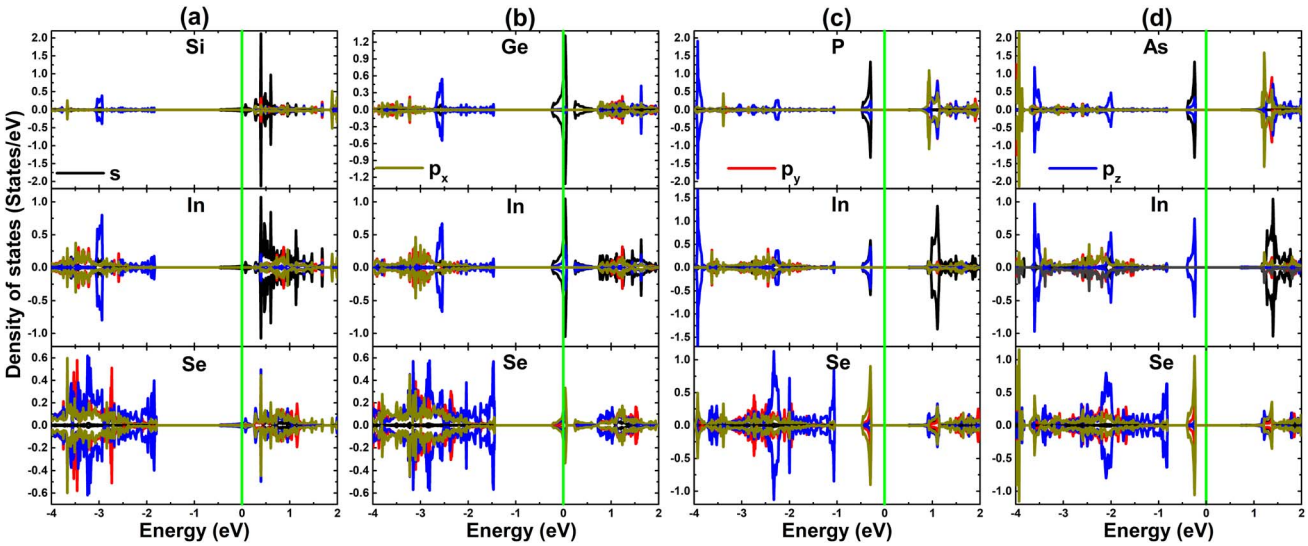

Fig. 4 Projected density of states of impurities and their nearest neighboring In and Se atoms in (a) Si_{In}@InSe, (b) Ge_{In}@InSe, (c) P_{In}@InSe, and (d) As_{In}@InSe monolayer (the Fermi level is set to 0 eV: green vertical line).

© 2025 The Author(s). Published by the Royal Society of Chemistry

Open Access Article. Published on 23 Jänner 2025. Downloaded on 25.02.2026 06:53:42.
This article is licensed under a Creative Commons Attribution-NonCommercial 3.0 Unported Licence.

calculated formation energies. Irrespective of the preferred doping site, all the n- and p-doped systems are investigated to clarify role of impurities. Once formed, all four X_{Se}@InSe systems are stabilized as suggested by their negative E_c values between −3.17 and −3.18 eV per atom.

Our spin-polarized calculations demonstrate the nonmagnetic nature of Si_{Se}@InSe and Ge_{Se}@InSe systems with zero magnetic moments, confirming the preservation of the nonmagnetic nature of the InSe monolayer upon doping with Si and Ge atoms. Meanwhile, doping with VA-group impurities produces an integer total magnetic moment of 1.00 μ_B in the InSe monolayer. The spin density in P_{Se}@InSe and As_{Se}@InSe systems is illustrated in Fig. 5. From the figure, one can see that spin surfaces are highly concentrated at P and As sites, respectively. These results evidence that magnetic moments are derived primarily from VA-group dopant atoms. Bader charge analysis is carried out to assert the charge acquisition by impurities when they are incorporated into the Se sublattice. Specifically, Si/Ge, P, and As atoms attract charge amounts of 0.16, 0.58, and 0.46*e* from the host monolayer, respectively.

Fig. 6 shows the calculated spin-polarized band structures of X_{Se}@InSe systems. Importantly, a perfect coincidence is observed for Si_{Se}@InSe and Ge_{Se}@InSe systems, respectively. In these cases, doping induces a new subband in the upper part of valence band and mid-gap flat energy branches above the Fermi level to reduce the monolayer band gap. Specifically, an energy gap of 0.83 eV is obtained for both systems, which represents a reduction of 41.13% compared to the pristine InSe monolayer. New mid-gap states are also produced by doping with P and As atoms that do not go cross the Fermi level. However they appear at different energy points (one below the spin-up Fermi level and the other above the spin-down Fermi level) resulting in spin polarization in the vicinity of the Fermi level. The band structure profiles evidence the magnetic semiconductor nature of P_{Se}@InSe and As_{Se}@InSe systems, which may be introduced as prospective spintronic candidates.[50] Our calculations provide

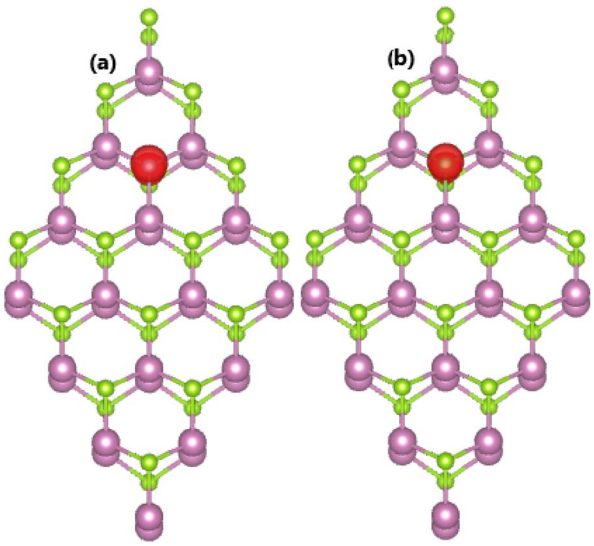

Fig. 5 Spin density (Iso-surface value of 0.005 *e* Å^{-3}) distributed in (a) P_{Se}@InSe and (b) As_{Se}@InSe systems.

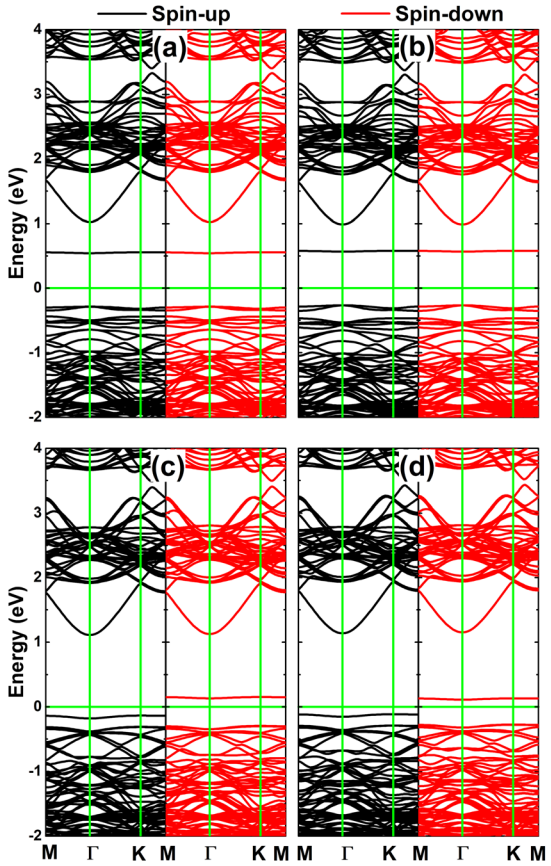

Fig. 6 Spin-polarized band structure of (a) Si_{Se}@InSe, (b) Ge_{Se}@InSe, (c) P_{Se}@InSe, and (d) As_{Se}@InSe monolayer (the Fermi level is set to 0 eV: green horizontal line).

spin-up/spin-down energy gaps of 1.25/0.43 and 1.25/0.39 eV for P_{Se}@InSe and As_{Se}@InSe systems, respectively.

PDOS spectra of impurities and their first (In) nearest neighboring atoms are given in Fig. 7 to further study the electronic structure and physical origin of magnetism. When doping with IVA-group atoms, X-$p_{x,y}$ states hybridize with In-$p_{x,y,z}$ states to form a subband in the upper part of the valence band, while the flat branches above the Fermi level primarily originate from X-p_z states. Meanwhile, the magnetic semiconductor nature of the P_{Se}@InSe and As_{Se}@InSe systems is mainly due to the p_z state of impurities since it generates mainly the flat energy states around the Fermi level, where a small contribution from In-$p_{x,y,z}$ states is also noted. The PDOS profile also evidences the important role of P-p_z and As-p_z states in producing the magnetism of P_{Se}@InSe and As_{Se}@InSe systems, respectively.

3.4 Effects of simultaneous doping at In + Se sublattices

Now, doping with pair dopant atoms is proposed to modify the InSe monolayer electronic and magnetic properties. The doped systems are named pX@InSe (X = Si, Ge, P, and As), where X1 and X2 refer to impurity incorporated at the In sublattice and Se sublattice, respectively. Applying eqn (3), E_f values of 3.06, 2.56, 2.75, and 2.32 eV are obtained for pSi@InSe, pGe@InSe,

Open Access Article. Published on 23 Jänner 2025. Downloaded on 25.02.2026 06:53:42.
This article is licensed under a Creative Commons Attribution-NonCommercial 3.0 Unported Licence.

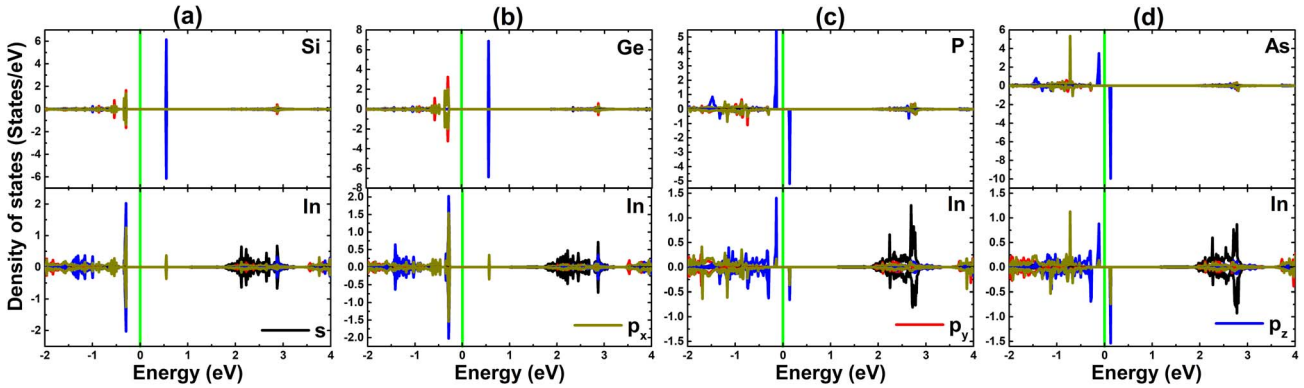

Fig. 7 Projected density of states of impurities and their nearest neighboring In atoms in (a) Si_{Se}@InSe, (b) Ge_{Se}@InSe, (c) P_{Se}@InSe, and (d) As_{Se}@InSe monolayer (the Fermi level is set to 0 eV: green vertical line).

pP@InSe, and pAs@InSe systems, respectively. The results indicate that doping with As–As pairs is energetically most favorable and easier to realize as compared with other cases.

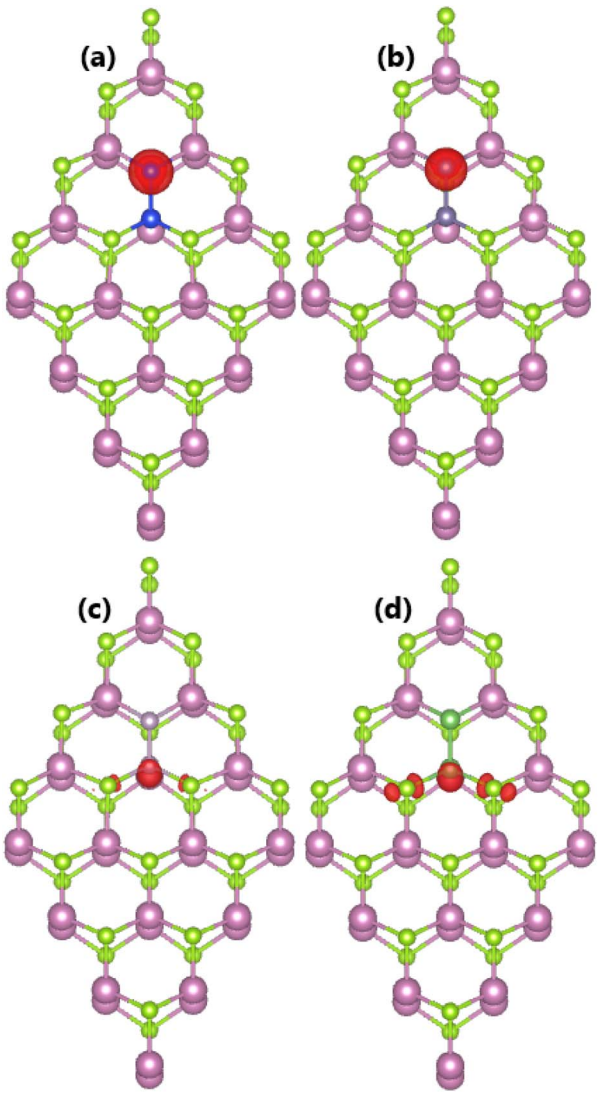

Fig. 8 Spin density (Iso-surface value of 0.005 e Å^{-3}) distributed in (a) pSi@InSe, (b) pGe@InSe, (c) pP@InSe, and (d) pAs@InSe systems.

The calculated (negative-feature) cohesive energies (see Table 1) suggest good structural and chemical stability of all four pX@InSe systems once they have been formed.

It is found that the InSe monolayer is magnetized by doping with pair IVA- and VA-group atoms, as confirmed by the nonzero magnetic moments. Specifically, integer total magnetic moments of 1.00 μ_B are obtained for pSi@InSe, pGe@InSe, and pAs@InSe systems, while a smaller value of 0.81 μ_B is obtained

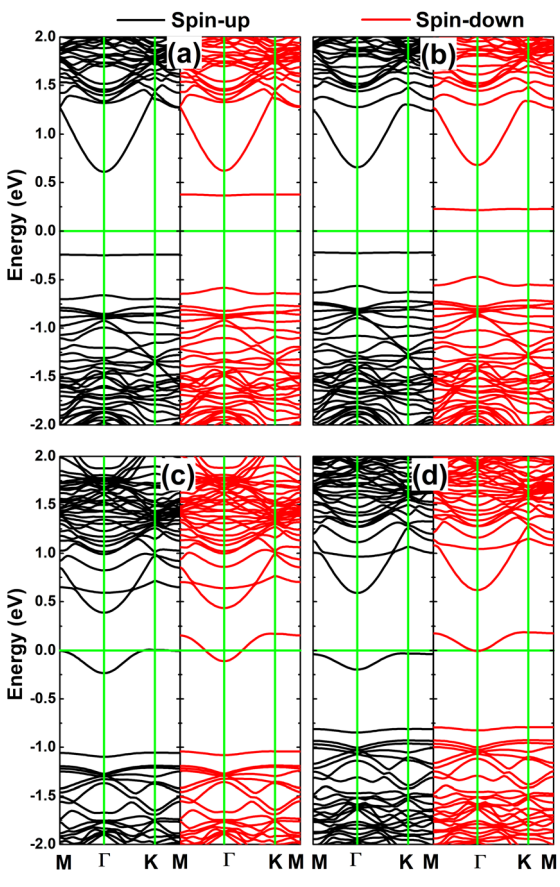

Fig. 9 Spin-polarized band structure of (a) pSi@InSe, (b) pGe@InSe, (c) pP@InSe, and (d) pAs@InSe systems (the Fermi level is set to 0 eV: green horizontal line).

© 2025 The Author(s). Published by the Royal Society of Chemistry

Open Access Article. Published on 23 Jänner 2025. Downloaded on 25.02.2026 06:53:42.
This article is licensed under a Creative Commons Attribution-NonCommercial 3.0 Unported Licence.

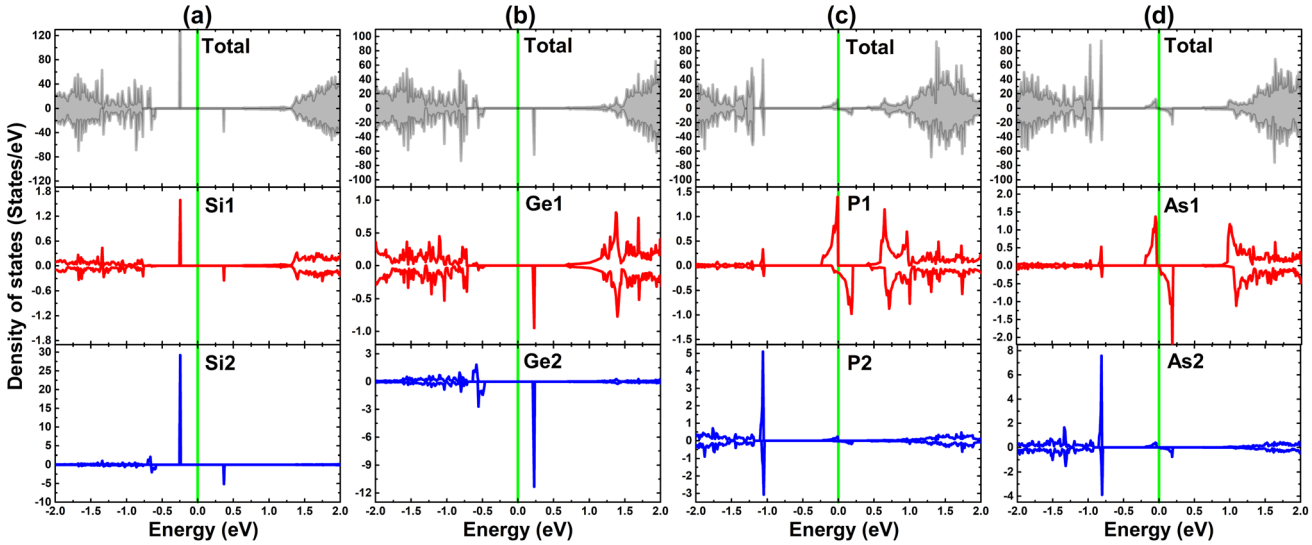

Fig. 10 Total density of states and atomic density of states of impurities of (a) pSi@InSe, (b) pGe@InSe, (c) pP@InSe, and (d) pAs@InSe systems (the Fermi level is set to 0 eV: Green vertical line).

for the pP@InSe system. Fig. 8 visualizes the spin density in pX@InSe systems, where different features are observed depending on the nature of impurities. A high concentration of spin surfaces indicates that magnetic moments of pSi@InSe and pGe@InSe systems are produced primarily by Si2 and Ge2 dopant atoms. Meanwhile, P1 and As1 impurities produce mainly the magnetic moments of pP@InSe and pAs@InSe systems, respectively, with a small contribution from their first nearest neighboring Se atoms. Furthermore, Bader charge analysis indicates that X1 impurities act as charge donors, while X2 dopant atoms are confirmed to act as charge acceptors. The calculated charge quantities are listed in Table 1.

Fig. 9 shows the calculated spin-polarized band structures of the InSe monolayer engineered by doping with pair atoms. In all cases, the spin-up and spin-down channels around the Fermi level show strong splitting with the appearance of new mid-gap energy branches, further reflecting the engineered magnetism. pSi@InSe and pGe@InSe are confirmed to be magnetic semiconductor systems since no energy branch overlaps with the Fermi level. In these cases, spin-up/spin-down states have energy gaps of 0.86/0.95 and 0.88/0.68 eV, respectively. In contrast, both spin states of the pP@InSe monolayer exhibit metallic character, confirming the monolayer metallization induced by doping with pair P atoms. On the other hand, metallic character is only observed for the spin-down state of the pAs@InSe monolayer, while the semiconductor spin-up state with an energy gap of 0.62 eV is obtained. These results evidence the half-metallicity of the pAs@InSe monolayer that is another desirable feature for spintronic applications.[51]

To further study the contribution of IVA- and VA-group impurities, the total density of states and their atom-decomposed density of states are given in Fig. 10. Focusing on the region around the Fermi level, it is noted that Si2 and Ge2 atoms mainly contribute to the mid-gap states of pSi@InSe and pAs@InSe systems, respectively. Meanwhile, in pP@InSe and pAs@InSe systems, the mid-gap states are formed primarily by the P1 and As1 dopant atoms to regulate the electronic nature of the systems, respectively. Strong spin splitting also confirms the role of Si2, Ge2, P1, and As1 in producing magnetism in respective pair-atoms-doped systems. Therefore, it can be concluded that the band structure and magnetism are engineered mainly by the mentioned impurities.

4. Conclusions

Using the spin-polarized DFT calculations, we developed a complete first-principles framework to investigate the feature-rich properties of IVA and VA group atom-doped InSe monolayers, including electronic band structures, projected density of states, and spin density distributions. The pristine InSe monolayer possesses good structural, dynamical, and thermal stability, exhibiting an indirect-gap semiconductor nature. Atom substitution generates new mid-gap energy states that determine the electronic and magnetic properties of the doped InSe monolayers. No magnetism is induced by n-type doping, where one electron doping metallizes the monolayer and two electron doping decreases significantly the monolayer's band gap. In these cases, the s states of impurities primarily contribute to formation of mid-gap states. Regarding the p-type doping process, two-hole doping results in a band gap reduction without magnetism, while one hole doping leads to a magnetic semiconductor nature with a total magnetic moment of 1.00 μ_B. Herein, the modification can be attributed mainly to the p_z state of the dopant atoms when forming mainly the band structure around the Fermi level. Interestingly, the substitution of pair IVA-group atoms makes new magnetic semiconductor materials with a total magnetic moment of 1.00 μ_B despite no magnetism being induced by a single impurity. The electronic and magnetic properties of the pSi@InSe and pGe@InSe systems are regulated primarily by the dopant atoms

© 2025 The Author(s). Published by the Royal Society of Chemistry

Open Access Article. Published on 23 Jänner 2025. Downloaded on 25.02.2026 06:53:42.
This article is licensed under a Creative Commons Attribution-NonCommercial 3.0 Unported Licence.

incorporated at the Se site. Meanwhile, impurities incorporated at In site determine the ground-state properties of pP@InSe and pAs@InSe systems that are confirmed to be magnetic metallic and half-metallic materials, respectively. Our study provides insights into the effects of doping sites on the electronic and magnetic properties of doped InSe monolayers, which can be used as valuable guidance to realize the functionalization of this 2D material towards multifunctional applications.

Data availability

Data related to this study are available upon reasonable request.

Conflicts of interest

The authors declare that they have no known competing financial interests or personal relationships that could have appeared to influence the work reported in this paper.

Acknowledgements

The calculations were performed at the DGCTIC-UNAM Supercomputing Center (projects LANCAD-UNAM-DGTIC-368).

References

1 J. Shim, H.-Y. Park, D.-H. Kang, J.-O. Kim, S.-H. Jo, Y. Park and J.-H. Park, Electronic and optoelectronic devices based on two-dimensional materials: From fabrication to application, *Adv. Electron. Mater.*, 2017, **3**(4), 1600364.
2 S. Kang, D. Lee, J. Kim, A. Capasso, H. S. Kang, J.-W. Park, C.-H. Lee and G.-H. Lee, 2D semiconducting materials for electronic and optoelectronic applications: potential and challenge, *2D Materials*, 2020, **7**(2), 022003.
3 M. Turunen, M. Brotons-Gisbert, Y. Dai, Y. Wang, E. Scerri, C. Bonato, K. D. Jöns, Z. Sun and B. D. Gerardot, Quantum photonics with layered 2D materials, *Nat. Rev. Phys.*, 2022, **4**(4), 219–236.
4 F. Xia, H. Wang, D. Xiao, M. Dubey and A. Ramasubramaniam, Two-dimensional material nanophotonics, *Nat. Photonics*, 2014, **8**(12), 899–907.
5 D. Deng, K. Novoselov, Q. Fu, N. Zheng, Z. Tian and X. Bao, Catalysis with two-dimensional materials and their heterostructures, *Nat. Nanotechnol.*, 2016, **11**(3), 218–230.
6 H. Li, J. Xiao, Q. Fu and X. Bao, Confined catalysis under two-dimensional materials, *Proc. Natl. Acad. Sci. U. S. A.*, 2017, **114**(23), 5930–5934.
7 X. Liu, T. Ma, N. Pinna and J. Zhang, Two-dimensional nanostructured materials for gas sensing, *Adv. Funct. Mater.*, 2017, **27**(37), 1702168.
8 M. Mathew, P. V. Shinde, R. Samal and C. S. Rout, A review on mechanisms and recent developments in pn heterojunctions of 2D materials for gas sensing applications, *J. Mater. Sci.*, 2021, **56**, 9575–9604.
9 D. Chimene, D. L. Alge and A. K. Gaharwar, Two-dimensional nanomaterials for biomedical applications: emerging trends and future prospects, *Adv. Mater.*, 2015, **27**(45), 7261–7284.
10 T. Hu, X. Mei, Y. Wang, X. Weng, R. Liang and M. Wei, Two-dimensional nanomaterials: fascinating materials in biomedical field, *Sci. Bull.*, 2019, **64**(22), 1707–1727.
11 Y. Xue, Q. Zhang, W. Wang, H. Cao, Q. Yang and L. Fu, Opening two-dimensional materials for energy conversion and storage: a concept, *Adv. Energy Mater.*, 2017, **7**(19), 1602684.
12 X. Zhang, L. Hou, A. Ciesielski and P. Samorì, 2D materials beyond graphene for high-performance energy storage applications, *Adv. Energy Mater.*, 2016, **6**(23), 1600671.
13 K. Rasool, R. P. Pandey, P. A. Rasheed, S. Buczek, Y. Gogotsi and K. A. Mahmoud, Water treatment and environmental remediation applications of two-dimensional metal carbides (MXenes), *Mater. Today*, 2019, **30**, 80–102.
14 T.-H. Le, Y. Oh, H. Kim and H. Yoon, Exfoliation of 2D materials for energy and environmental applications, *Chem.–Eur. J.*, 2020, **26**(29), 6360–6401.
15 K. S. Novoselov, A. K. Geim, S. V. Morozov, D.-e. Jiang, Y. Zhang, S. V. Dubonos, I. V. Grigorieva and A. A. Firsov, Electric field effect in atomically thin carbon films, *science*, 2004, **306**(5696), 666–669.
16 C. Soldano, A. Mahmood and E. Dujardin, Production, properties and potential of graphene, *Carbon*, 2010, **48**(8), 2127–2150.
17 M. J. Allen, V. C. Tung and R. B. Kaner, Honeycomb carbon: a review of graphene, *Chem. Rev.*, 2010, **110**(1), 132–145.
18 Y.-W. Son, M. L. Cohen and S. G. Louie, Energy gaps in graphene nanoribbons, *Phys. Rev. Lett.*, 2006, **97**(21), 216803.
19 J. E. Johns and M. C. Hersam, Atomic covalent functionalization of graphene, *Acc. Chem. Res.*, 2013, **46**(1), 77–86.
20 M. Chhowalla, Z. Liu and H. Zhang, Two-dimensional transition metal dichalcogenide (TMD) nanosheets, *Chem. Soc. Rev.*, 2015, **44**(9), 2584–2586.
21 X. Duan, C. Wang, A. Pan, R. Yu and X. Duan, Two-dimensional transition metal dichalcogenides as atomically thin semiconductors: opportunities and challenges, *Chem. Soc. Rev.*, 2015, **44**(24), 8859–8876.
22 Y. Wei, P. Zhang, R. A. Soomro, Q. Zhu and B. Xu, Advances in the synthesis of 2D MXenes, *Adv. Mater.*, 2021, **33**(39), 2103148.
23 D. Ayodhya, A review of recent progress in 2D MXenes: Synthesis, properties, and applications, *Diamond Relat. Mater.*, 2023, **132**, 109634.
24 K. Khan, A. K. Tareen, Q. U. Khan, M. Iqbal, H. Zhang and Z. Guo, Novel synthesis, properties and applications of emerging group VA two-dimensional monoelemental materials (2D-Xenes), *Mater. Chem. Front.*, 2021, **5**(17), 6333–6391.
25 H. Şahin, S. Cahangirov, M. Topsakal, E. Bekaroglu, E. Akturk, R. T. Senger and S. Ciraci, Monolayer honeycomb structures of group-iv elements and iii-v binary compounds: First-principles calculations, *Phys. Rev. B:Condens. Matter Mater. Phys.*, 2009, **80**(15), 155453.
26 F. Ersan, D. Keçik, V. Özçelik, Y. Kadioglu, O. Ü. Aktürk, E. Durgun, E. Aktürk and S. Ciraci, Two-dimensional pnictogens: A review of recent progresses and future

© 2025 The Author(s). Published by the Royal Society of Chemistry

Open Access Article. Published on 23 Jänner 2025. Downloaded on 25.02.2026 06:53:42.
This article is licensed under a Creative Commons Attribution-NonCommercial 3.0 Unported Licence.

research directions, *Applied Physics Reviews*, 2019, **6**(2), 021308.
27 C. V. Ha, L. Ha, D. K. Nguyen, D. T. Anh, J. Guerrero-Sanchez, D. Hoat, *et al.*, First-principles study of SiC and GeC monolayers with adsorbed non-metal atoms, *RSC Adv.*, 2023, **13**(22), 14879–14886.
28 H. L. Zhuang, A. K. Singh and R. G. Hennig, Computational discovery of single-layer III-V materials, *Phys. Rev. B:Condens. Matter Mater. Phys.*, 2013, **87**(16), 165415.
29 X.-F. Liu, Z.-J. Luo, X. Zhou, J.-M. Wei, Y. Wang, X. Guo, B. Lv and Z. Ding, Structural, mechanical, and electronic properties of 25 kinds of III–V binary monolayers: A computational study with first-principles calculation, *Chin. Phys. B*, 2019, **28**(8), 086105.
30 H. Wang, G. Qin, J. Yang, Z. Qin, Y. Yao, Q. Wang and M. Hu, First-principles study of electronic, optical and thermal transport properties of group III–VI monolayer MX (M= Ga, In; X= S, Se), *J. Appl. Phys.*, 2019, **125**(24), 245104.
31 S. Demirci, N. Avazlı, E. Durgun and S. Cahangirov, Structural and electronic properties of monolayer group III monochalcogenides, *Phys. Rev. B*, 2017, **95**(11), 115409.
32 J. Chen, X. Tan, P. Lin, B. Sa, J. Zhou, Y. Zhang, C. Wen and Z. Sun, Comprehensive understanding of intrinsic mobility in the monolayers of III–VI group 2D materials, *Phys. Chem. Chem. Phys.*, 2019, **21**(39), 21898–21907.
33 G. W. Mudd, S. A. Svatek, T. Ren, A. Patanè, O. Makarovsky, L. Eaves, P. H. Beton, Z. D. Kovalyuk, G. V. Lashkarev, Z. R. Kudrynskyi, *et al.*, Tuning the bandgap of exfoliated InSe nanosheets by quantum confinement, *Adv. Mater.*, 2013, **25**(40), 5714.
34 E. Petroni, E. Lago, S. Bellani, D. W. Boukhvalov, A. Politano, B. Gürbulak, S. Duman, M. Prato, S. Gentiluomo, R. Oropesa-Nuñez, *et al.*, Liquid-phase exfoliated indium–selenide flakes and their application in hydrogen evolution reaction, *Small*, 2018, **14**(26), 1800749.
35 H.-C. Chang, C.-L. Tu, K.-I. Lin, J. Pu, T. Takenobu, C.-N. Hsiao and C.-H. Chen, Synthesis of large-area InSe monolayers by chemical vapor deposition, *Small*, 2018, **14**(39), 1802351.
36 J. Zhou, J. Shi, Q. Zeng, Y. Chen, L. Niu, F. Liu, T. Yu, K. Suenaga, X. Liu, J. Lin, *et al.*, InSe monolayer: synthesis, structure and ultra-high second-harmonic generation, *2D Materials*, 2018, **5**(2), 025019.
37 C. Zhang, X. Chen, B. Cao, H. Duan, Q. Sun and F. Ouyang, Tuning the band gap of the InSe monolayer by substitutional doping, *Appl. Surf. Sci.*, 2022, **579**, 152190.
38 W. Ju, T. Li, Q. Zhou, H. Li, X. Li and D. Ma, Adsorption of 3d transition-metal atom on InSe monolayer: a first-principles study, *Comput. Mater. Sci.*, 2018, **150**, 33–41.
39 V.-T. Pham and T.-H. Fang, Effects of temperature and intrinsic structural defects on mechanical properties and thermal conductivities of InSe monolayers, *Sci. Rep.*, 2020, **10**(1), 15082.
40 W. Kohn and L. J. Sham, Self-consistent equations including exchange and correlation effects, *Phys. Rev.*, 1965, **140**(4A), A1133.
41 G. Kresse and J. Furthmüller, Efficiency of *ab initio* total energy calculations for metals and semiconductors using a plane-wave basis set, *Comput. Mater. Sci.*, 1996, **6**(1), 15–50.
42 G. Kresse and J. Furthmüller, Efficient iterative schemes for *ab initio* total-energy calculations using a plane-wave basis set, *Phys. Rev. B:Condens. Matter Mater. Phys.*, 1996, **54**(16), 11169.
43 J. P. Perdew, K. Burke and M. Ernzerhof, Generalized gradient approximation made simple, *Phys. Rev. Lett.*, 1996, **77**(18), 3865.
44 T. M. Project, Materials data on InSe by materials project, DOI: **10.17188/1195613**.
45 H. J. Monkhorst and J. D. Pack, Special points for Brillouin-zone integrations, *Phys. Rev. B:Condens. Matter Mater. Phys.*, 1976, **13**(12), 5188.
46 A. Togo, L. Chaput, T. Tadano and I. Tanaka, Implementation strategies in phonopy and phono3py, *J. Phys.:Condens. Matter*, 2023, **35**(35), 353001, DOI: **10.1088/1361-648X/acd831**.
47 S. Nosé, A unified formulation of the constant temperature molecular dynamics methods, *J. Chem. Phys.*, 1984, **81**(1), 511–519.
48 W. G. Hoover, Canonical dynamics: Equilibrium phase-space distributions, *Phys. Rev. A:At., Mol., Opt. Phys.*, 1985, **31**(3), 1695.
49 A. V. Krukau, O. A. Vydrov, A. F. Izmaylov and G. E. Scuseria, Influence of the exchange screening parameter on the performance of screened hybrid functionals, *J. Chem. Phys.*, 2006, **125**(22), 224106.
50 X. Li and J. Yang, First-principles design of spintronics materials, *Natl. Sci. Rev.*, 2016, **3**(3), 365–381.
51 X. Li and J. Yang, Low-dimensional half-metallic materials: theoretical simulations and design, *Wiley Interdiscip. Rev.: Comput. Mol. Sci.*, 2017, **7**(4), e1314.

© 2025 The Author(s). Published by the Royal Society of Chemistry